INSTITUTE FOR FUSION STUDIES

DOE/ET-53088-567 IFSR #567

Particle Simulations in Toroidal Geometry

A.Y. AYDEMIR
Institute for Fusion Studies
The University of Texas at Austin
Austin, Texas 78712

September 1992

THE UNIVERSITY OF TEXAS

AUSTIN

Particle Simulations in Toroidal Geometry

A.Y. Aydemir
Institute for Fusion Studies
The University of Texas at Austin
Austin, Texas 78712

Abstract

A computational tool to be used in kinetic simulations of toroidal plasmas is being developed. The initial goal of the project is to develop an electrostatic gyrokinetic model for studying transport and stability problems in tokamaks. In this brief report, preliminary results from the early stages of this effort are presented.

Presented at the IAEA Technical Committee Meeting on Advances in Simulation and Modelling of Thermonuclear Plasmas
Montréal, June 15-17, 1992.

I. Introduction

Gyrofluid and gyrokinetic models are emerging as two powerful tools for studying plasmas in present and future devices in the magnetic fusion program. Many successful examples of these approaches and their application to the study of transport in tokamaks have been presented at this workshop.[1, 2, 3] This brief article summarizes our efforts, at this point more pedagogical than investigative, in developing a tool for kinetic simulations of toroidal devices. The following sections present results from our evolving computational model, starting with full dynamics electrons and ions, and ending with a drift kinetic description of electrons using "low-noise" techniques.

II. Full Dynamics Particles — Nonmagnetized Plasma

As a starting point, an electrostatic model with unmagnetized particles, but with the full geometric effects of a toroidal geometry is chosen. Motivated by a desire to work in a system that is most appropriate to the task at hand, a mixture of coordinate systems are used (Fig. 1). Particles are pushed in an (x, y, z) Cartesian coordinate system; gather/scatter operations are performed in the toroidal (r, θ, ζ) system, where r is the radial coordinate, and θ, ζ are the poloidal and toroidal angles, respectively. A mixed (r, m, n) system, where m, n are the poloidal and toroidal Fourier mode numbers, respectively, is used when solving for the fields. Transformations between (x, y, z) and (r, θ, ζ) systems involve simple rotations. Fast Fourier Transform (FFT) routines are used for transformations between (r, θ, ζ) and (r, m, n) systems. The three-dimensional weight functions for the particles are taken to be tensor product of one dimensional splines: $S(\mathbf{r} - \mathbf{r}_j) = S_r(r - r_j)S_\theta(\theta - \theta_j)S_\zeta(\zeta - \zeta_j)$, where S_r, S_θ, and S_ζ are $1D$ splines of up to $5th$ order.[4] These higher order splines are being tested for their low noise characteristics and their ability to reduce aliasing errors.

In early tests of various parts of the code, such as gather/scatter routines, and the Poisson solver, a rather artificial distribution of particles is used as in initial condition: Cold electrons and ions are uniformly distributed in two concentric rings, as shown in Fig. (2a). In cylindrical geometry with poloidal and axial symmetry, the inner ring composed of electrons is expected to expand in radius very rapidly, pass through the outer ring composed of ions, get reflected by the circular wall, and eventually collapse to nearly its original size. In the absence of any symmetry breaking errors, this process is expected to repeat itself until collisional damping between the electrons and ions slows down the rapid radial oscillations of the electron ring. Note, however, that the system is highly unstable; any perturbation of either ring will prevent the symmetric collapse of the electron ring to its original configuration, causing the electrons to fly apart in essentially random directions. The highly unstable nature of this electrostatic system makes it particularly useful as a diagnostic tool. Figures 2(a–f) show the two rings at various points during one cycle of this process. Also shown are the radial profiles of the electrostatic potential at the given times. For this test run, some of the relevant parameters were as follows: N (the number of particles) $= 6400$, $T_e = T_i = 0$, and $m_i/m_e = 100$. A $32 \times 16 \times 16$ grid was used. The order of the splines were $3 \times 5 \times 5$ (radial, poloidal, and toroidal directions, respectively). Figures 3(a,b) show the time histories of the electric field and kinetic energies in the system. Three complete periods of the radial oscillations of the electron ring are shown; note that the ions are essentially stationary on this time scale. The minima in the electric field energy occur when the electrons pass through the ion ring, twice each period. The local minimum in the kinetic energy occurs during the electron ring's reflection by the wall; the absolute minimum occurs when the ring collapses down to its minimum radius. If there are any symmetry breaking computational errors, the ring is lost during its first collapse; thus, survival of the system for three complete cycles validates various components of the electrostatic, unmagnetized model.

III. Full Dynamics Particles — Magnetized Plasma

For a magnetized model, an important issue is the code's ability to follow particle trajectories in a toroidal magnetic field. Since the tests performed in the previous section effectively checked the response to collective effects, here results from a number of single particle tests are presented. Figure 4 demonstrates the ability of the code to accurately follow the toroidal particle trajectories, and to deal with the coordinate singularity at $r = 0$ and the boundary conditions at the circular wall. Figure (4a) shows a banana orbit, the projection onto the poloidal plane of a trapped particle orbit (with parameters deliberately chosen so as to make it resemble an $m = 1$ island!). Figure (4b) shows a similar orbit that passes near the coordinate axis, $r = 0$. For the same orbit, time history of the canonical angular momentum, $p_\zeta = m_j q_j v_\zeta + \Omega_e q_j \psi$, where $\psi = g A_\zeta$, and $g = 1 + \epsilon r \cos\theta$, is shown in Fig. (4c); maximum relative change in p_ζ is approximately 0.7% for this particularly sensitive orbit passing near the origin. Finally, Fig. (4d) shows the behaviour of a particle that drifts into the wall and then bounces along it. The boundary conditions applied are those of Naitou, *et al.*,[5] which involve reflection of the components of the velocity normal to the magnetic field.

More out of curiosity than for its diagnostic value, the "ring dynamics" of the previous section is reexamined in the presence of toroidal and poloidal magnetic fields. Not surprisingly, it is found that the fields do confine particles, as the radial oscillations of the unmagnetized electron ring are not observed here. Unfortunately, although the electron ring survives for quite a bit longer than in the unmagnetized case, it is still eventually destroyed, this time by an apparent instability driven by the $\mathbf{E} \times \mathbf{B}$ rotation of the ring.[6] Figure 5 shows the rings and the radial profile of the electrostatic potential at various times during the development of this instability. The calculation was performed in a torus with $\epsilon = 1/3$; a $32 \times 16 \times 16$ mesh, and $3 \times 5 \times 5-$order splines were used. Some of the other parameters were: $N = 25600$, $m_i/m_e = 100$, $T_i = T_e = 0$, and $\omega_{pe} = \Omega_e = 1$.

IV. Drift-Kinetic Electrons

The next logical step in the development of a practical computational tool for studying stability and transport in toroidal devices seems to be the removal of time and spatial scales associated with the electron gyromotion by using a guiding-center description of the electrons, where the particle orbits are determined by the following equations, suitably normalized:

$$\frac{d\mathbf{x}}{dt} = v_{\|}\hat{\mathbf{b}} + \mathbf{v}_D \ , \tag{1}$$

$$\mathbf{v}_D = \frac{\omega_{pe}^2}{\Omega_e}\,\frac{\mathbf{B}\times\boldsymbol{\nabla}\phi}{B^2} + \frac{1}{\Omega_e}\,\frac{m}{q}\left[\frac{\mu B}{m} + v_{\|}^2\right]\frac{\mathbf{B}\times\boldsymbol{\nabla}B}{B^3} \ , \quad \text{and} \tag{2}$$

$$m\,\frac{dv_{\|}}{dt} = \omega_{pe}^2 q\,E_{\|} - mu\nabla_{\|}B \ . \tag{3}$$

The resulting system is solved with a commonly-used modified Euler scheme.[7] Figure 6 compares a test-particle guiding center banana orbit (solid line) with that of a full-dynamics electron. The agreement is quite good; the small discrepancy near the turning points can be attributed to the fact that full-dynamics electron samples a finite volume of space with a varying magnetic field, which becomes significant when $v_{\|} \simeq 0$ (an FLR effect). Further comparisons are made in the next section.

V. Implementation of the δf Algorithm

The full-dynamics and the drift-kinetic models of the previous sections have also been formulated in terms of the low-noise "δf" algorithm.[8, 9] For this purpose, the drift kinetic equation is written in the form

$$\frac{df}{dt} = \frac{\partial f}{\partial t}(v_{\|}\hat{\mathbf{b}} + \mathbf{v}_D)\cdot\frac{\partial f}{\partial \mathbf{x}} + \frac{dv_{\|}}{dt}\,\frac{\partial f}{\partial v_{\|}} = 0 \ . \tag{4}$$

Then letting $f = f_0 + \delta f$, where f_0 is chosen to be a local Maxwellian, the nonlinear

equation for δf can be put in the form

$$\frac{d}{dt}\left(\frac{\delta f}{f_0}\right) = \left[1+\left(\frac{\delta f}{f_0}\right)\right]\left[\frac{\omega_{pe}^2}{v_{th}^2}\,\frac{q}{m} v_{\|} E_{\|} + \frac{\mu}{T_0}\,\mathbf{v}_E\cdot\boldsymbol{\nabla} B\right]\,, \tag{5}$$

where $\mathbf{v}_E = (\omega_{pe}^2/\Omega_e)\mathbf{B}\times\boldsymbol{\nabla}\phi/B^2$. Equation 5 is solved along the characteristics defined by Eqs. (1)–(3). Note that at this stage, both density and temperature gradients are ignored.

Similarly, the following nonlinear equation is obtained for the full-dynamics ions

$$\frac{d}{dt}\left(\frac{\delta f}{f_0}\right) = \left[1+\left(\frac{\delta f}{f_0}\right)\right]\frac{\omega_{pe}^2}{v_{th}^2}\,\frac{q}{m}\,\mathbf{v}\cdot\mathbf{E}\,, \tag{6}$$

which is solved along the usual characteristics given by $d\mathbf{x}/dt = \mathbf{v}$, and $d\mathbf{v}/dt = q/m(\omega_{pe}^2\mathbf{E} + \Omega_e\mathbf{v}\times\mathbf{B})$.

The resulting equations for both electrons and ions are again time-advanced with a predictor-corrector scheme.[7]

The time evolution of the electric field and kinetic energies from three different models are presented in Fig. 7. The calculations are done in a torus with $\epsilon = 1/3$; again a $32\times16\times16$ grid with $3\times3\times3-$ order splines are used. The number of particles per cell is approximately one ($N = 9968$), and $\omega_{pe} = \Omega_e = 1$, $m_i/m_e = 100$, and $\Delta t = 0.4$. The initial distribution function is a Maxwellian with uniform density and temperature. The results in Fig. 7a are from a model with full-dynamics electrons and ions, where the particles are advanced with a leap-frog scheme. The same calculation is repeated in Fig. 7b with the δf algorithm. As it is commonly observed with this low-noise technique, the fluctuation energy is many orders of magnitude lower than in the conventional approach. Finally, in Fig. 7c, the δf algorithm is applied to drift-kinetic electrons. The full-dynamics calculations (Fig. 7a,b) exhibit a slow, linear increase in the kinetic energy over time (usually labelled "self-heating"). The filtering techniques that prevent this process[10] have not been implemented yet. An opposite problem occurs in the guiding-center calculations that use the modified-Euler scheme; the slow "cooling" observed here (0.2% over 5000 time-steps) is probably due to the slightly dissipative nature of the two-step predictor-corrector algorithm.

VI. Summary

Preliminary results from an evolving series of kinetic models of toroidal particle simulations are described. Starting point is a full-dynamics, electrostatic model that follows the gyromotion of both ions and electrons in toroidal geometry, with a zero-β toroidal equilibrium field. The progress to date includes a guiding-center electron model that treats both species with the low-noise δf algorithm. Work is underway to include density and temperature gradients in the equilibrium, and to implement a gyrokinetic description of the ions. The immediate goal of the project is the development of an efficient electrostatic gyrokinetic model that can be used to study transport and stability in tokamaks.

Acknowledgments

The author acknowledges many useful discussions with participants at the meeting; in particular, suggestions of V. Decyk and C. Birdsall on the self-heating problem are greatly appreciated. The author also thanks Dr. Magdi Shoucri for his enormous patience and tolerance of the delay in the preparation of this manuscript. This work was supported by the U.S. Department of Energy under contract No. DE-FG05-80ET-53088.

References

[1]S. Parker *et al.*, "Status and prospects for gyrokinetic simulation models for tokamak plasmas", IAEA Technical Committee Meeting on Advances in Simulation and Modelling of Thermonuclear Plasmas, Montréal, June 15-17 (1992), See also W.W. Lee, "Gyrokinetic Particle Simulation Model," J. Comp. Phys. **72**, 243 (1987).

[2]A. Dimits *et al.*, "Simulation models for tokamak plasmas", *ibid.* See also A.M. Dimits and W.W. Lee, "Partially linearized algorithms in gyrokinetic particle simulation," Princeton University PPPL-2718 (October 1990).

[3]G.W. Hammett, "Advances in the incorporation of kinetic effects in fluid simulation of plasmas", *ibid.* See also G.W Hammett, W. Dorland, and F.W. Perkins, "Fluid models of phase mixing, Landau damping, and nonlinear gyrokinetic dynamics," Phys. Fluids B **4**, 2052 (1992).

[4]Hirotada Abe, Natsuhiko Sakairi, and Ryohei Itatani, J. Comp. Phys. **63**, 247 (1986).

[5]H. Naitou, S. Tokuda, and T. Kamimura, J. Comp. Phys. **33**, 86 (1979).

[6]The author was told by J. Dawson and C.K. Birdsall at the meeting that this is the well-known "diocotron" instability.

[7]C.Z. Cheng and H.Okuda, J. Comp. Phys. **25**, 133 (1977).

[8]T. Tajima and F.W. Perkins, Proceedings of the Sherwood Theory Conference, paper 2P9, Baltimore, MD (1983).

[9]M. Kotschenreuther, Bull. Am. Phys. Soc. **34**, 2107 (1988).

[10]Charles K. Birdsall and A. Bruce Langdon, *Plasma Physics via Computer Simulations*, McGraw-Hill (1985).

Figure Captions

1. The Cartesian and toroidal coordinate systems used in the calculations.

2. The evolution of the unmagnetized electron and ion rings in cylindrical geometry. The radial profiles of the electrostatic potential are also shown at the given times. This highly unstable system is used in testing of gather/scatter and field-solver routines.

3. Time history of the electric field and kinetic energy during three periods of the radial oscillations of the electron ring.

4. Test particle orbits: a) and b) show banana orbits with different initial conditions. c) shows the time history of the toroidal canonical angular momentum for the orbit in b), which passes near the coordinate axis, $r = 0$. d) shows the orbit of a particle that drifts into the wall.

5. The evolution of the magnetized rings in toroidal geometry, showing the eventual break-up of the electron ring due to a diocotron instability.

6. Comparison of banana orbits traced out by full-dynamics and guiding-center particles.

7. Time history of the electric field and kinetic energies for three different models: a) Full-dynamics ions and electrons, b) full dynamics particles with the δf algorithm, c) drift-kinetic electrons with the δf algorithm.

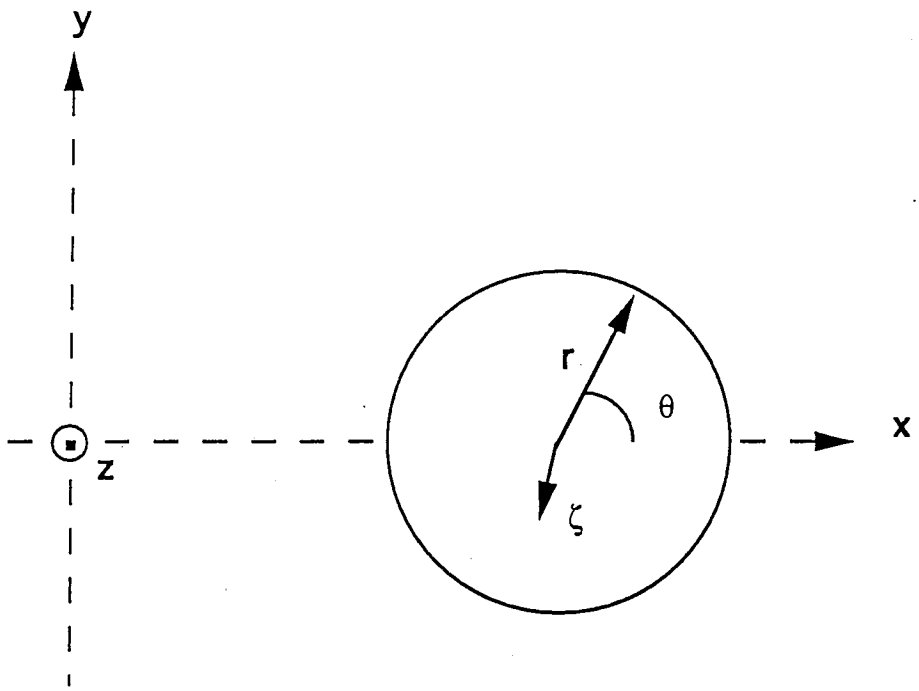

Fig. 1

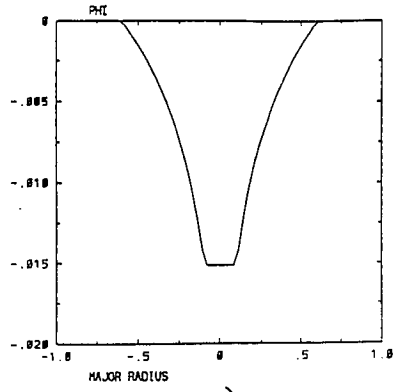

a)

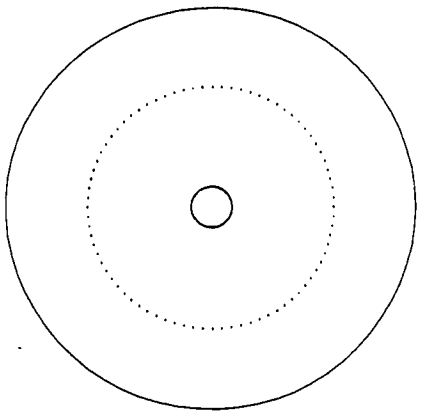

t=1.00000E-01 zt= .000 PARTICLE POS.

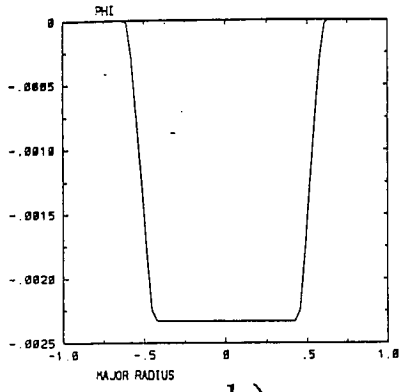

b)

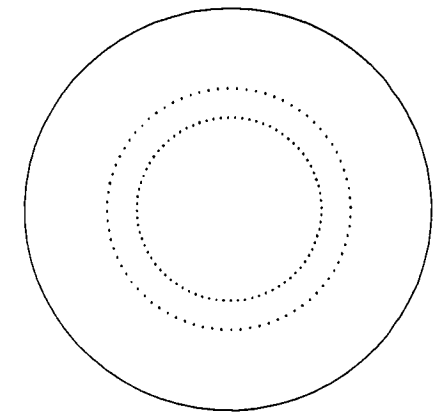

t=5.10000E+00 zt= .000 PARTICLE POS.

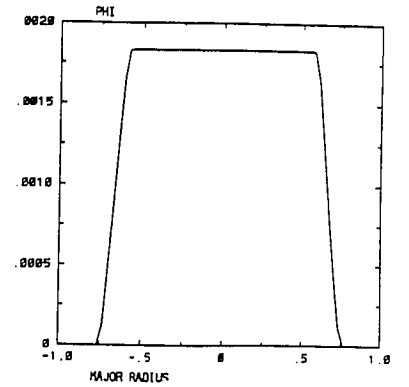

c)

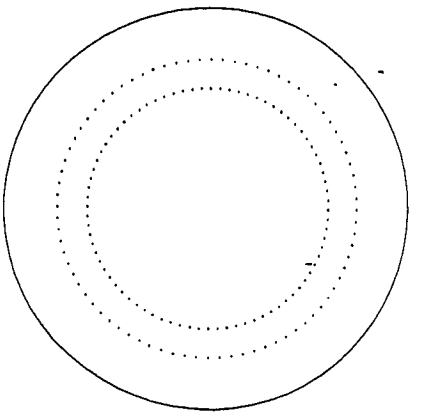

t=7.60000E+00 zt= .000 PARTICLE POS.

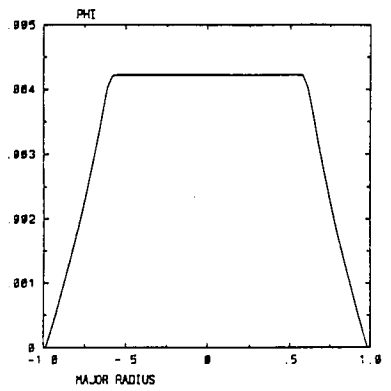

d)

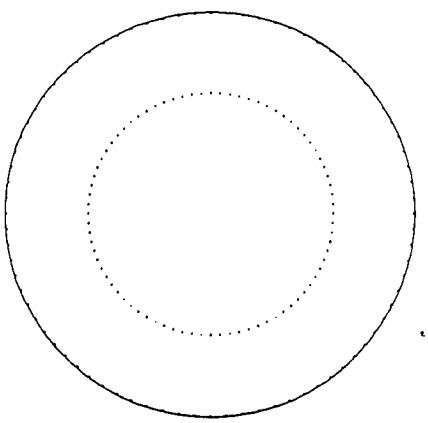

t=1.01000E+01 zt= .000 PARTICLE POS.

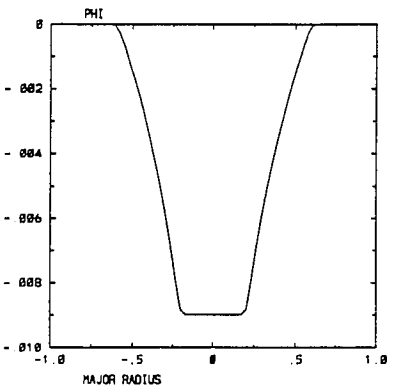

e)

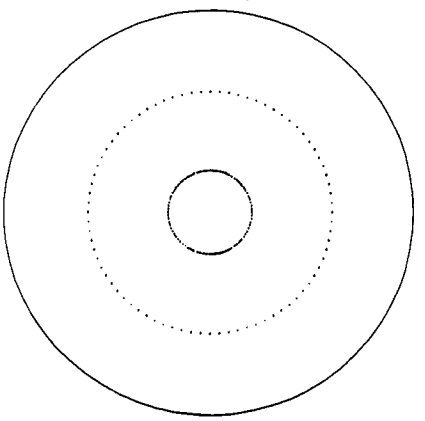

t=1.76000E+01 zt= .000 PARTICLE POS.

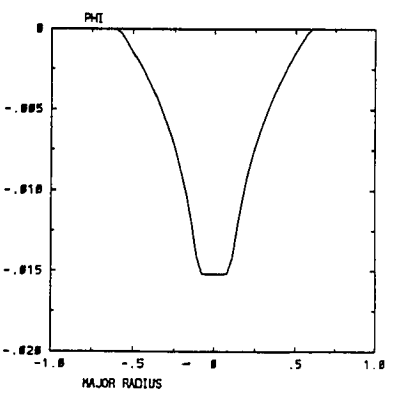

f)

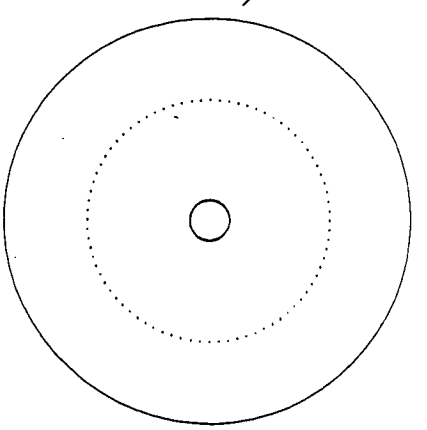

t=2.01000E+01 zt= .000 PARTICLE POS.

Fig. 2

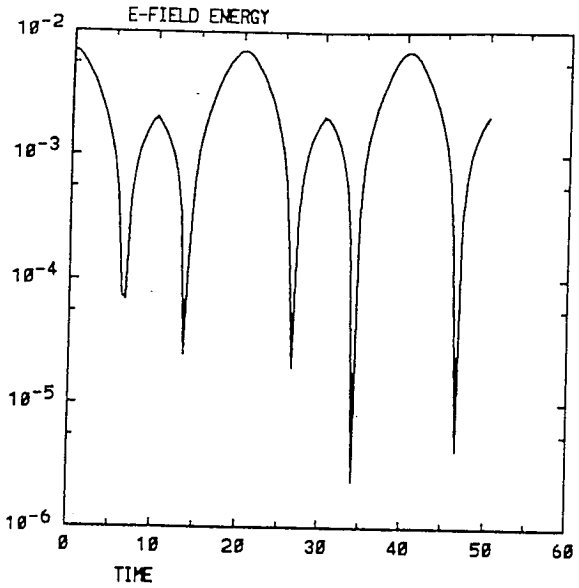
E-FIELD ENERGY
10^-2
10^-3
10^-4
10^-5
10^-6
0
10
20
30
40
50
60
TIME

a)

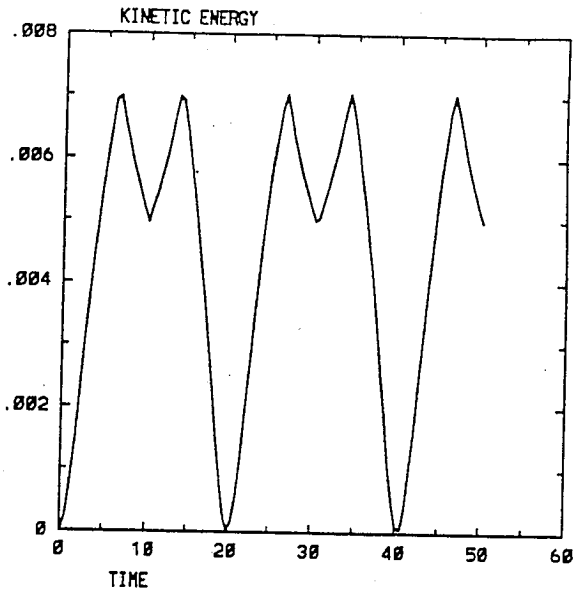
KINETIC ENERGY
.008
.006
.004
.002
0
0
10
20
30
40
50
60
TIME

b)

Fig. 3

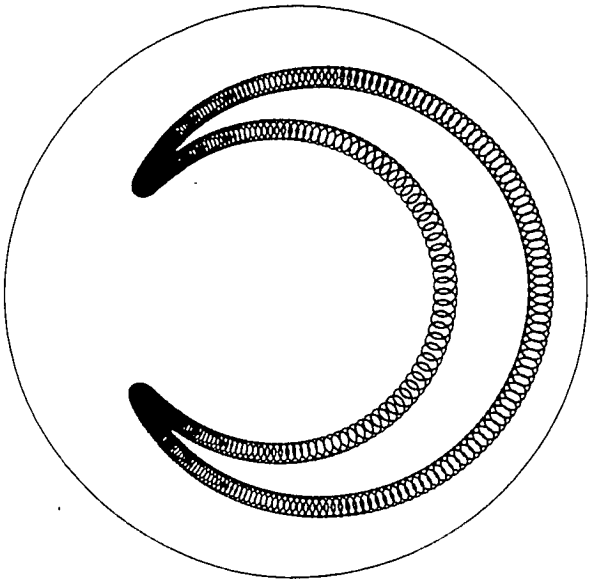

a)

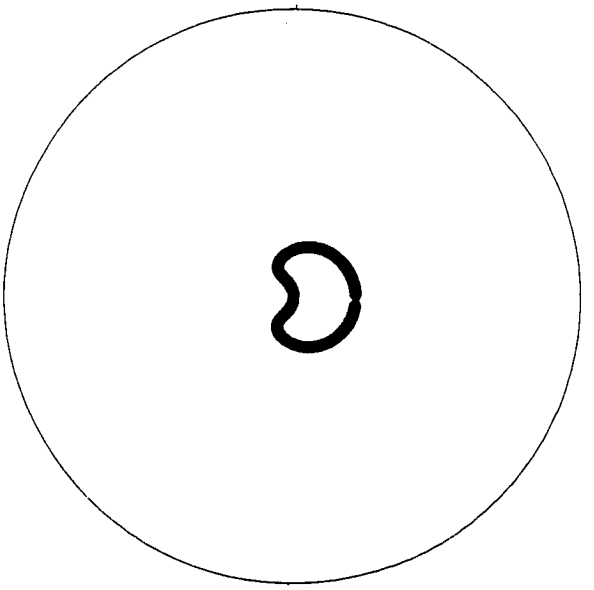

b)

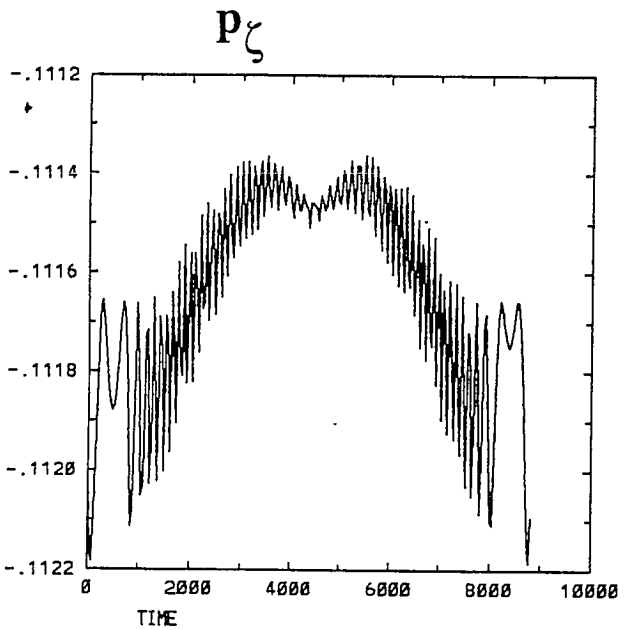
p_ζ
-.1112
-.1114
-.1116
-.1118
-.1120
-.1122
0
2000
4000
6000
8000
10000
TIME

c)

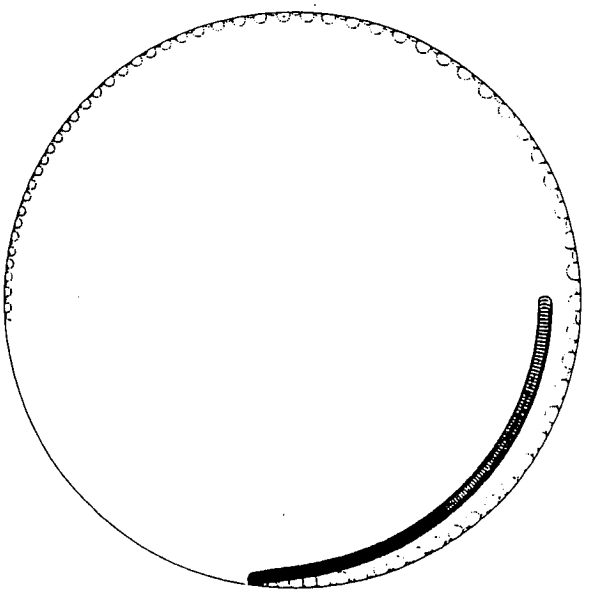

d)

Fig. 4

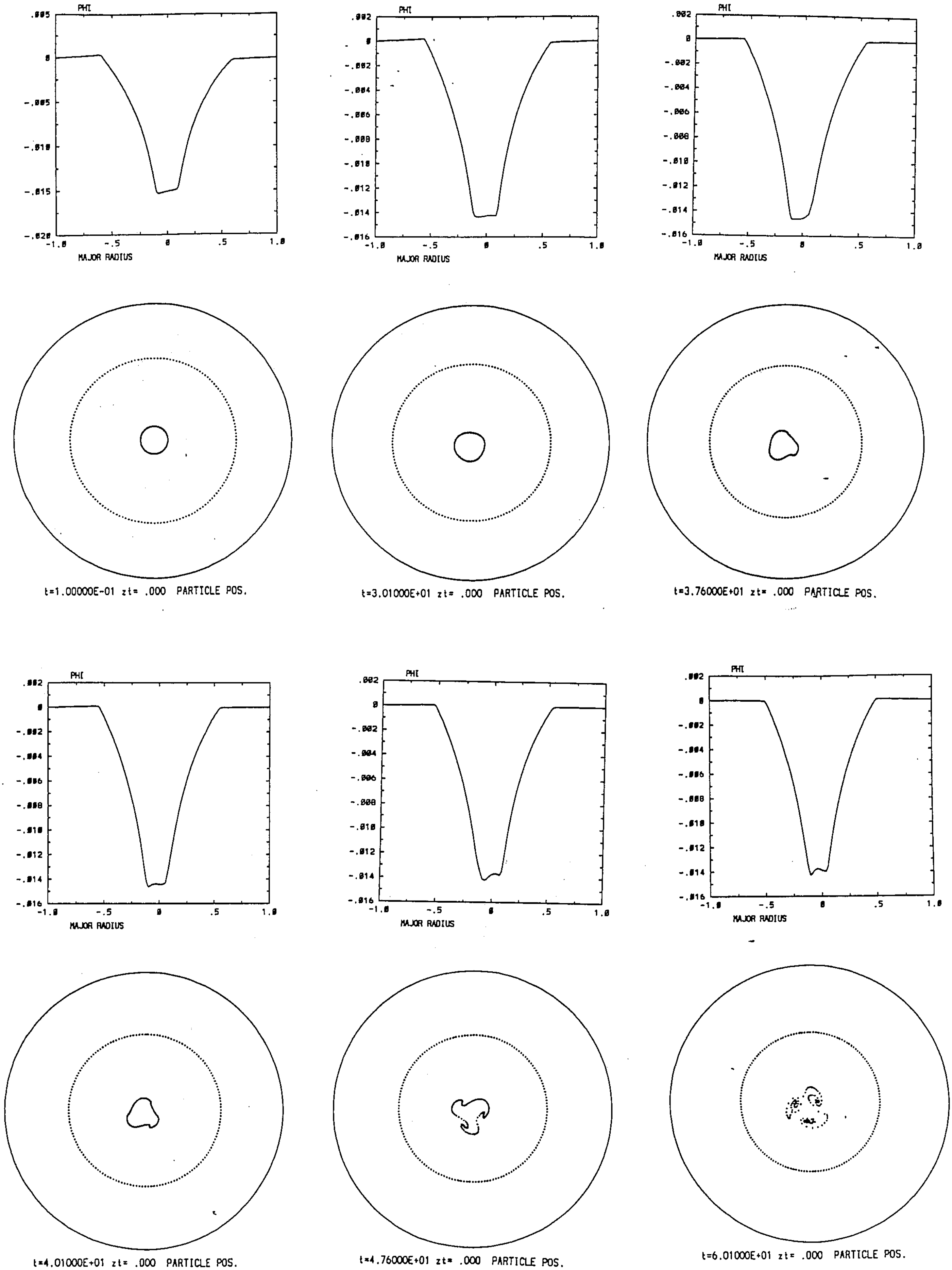
PHI
MAJOR RADIUS
t=1.00000E-01 zt= .000 PARTICLE POS.
t=3.01000E+01 zt= .000 PARTICLE POS.
t=3.76000E+01 zt= .000 PARTICLE POS.
t=4.01000E+01 zt= .000 PARTICLE POS.
t=4.76000E+01 zt= .000 PARTICLE POS.
t=6.01000E+01 zt= .000 PARTICLE POS.

Fig. 5

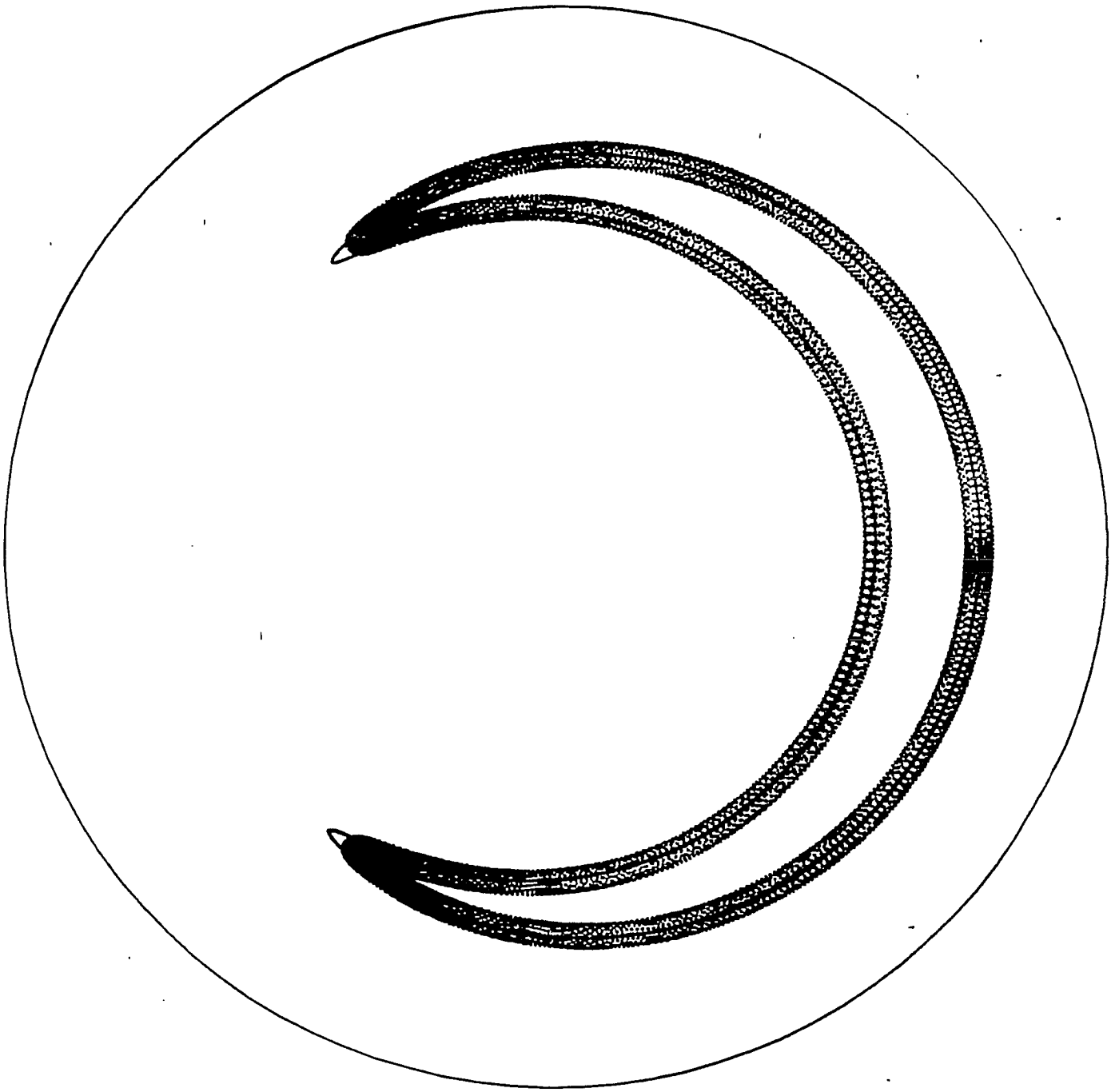

Fig. 6

a)

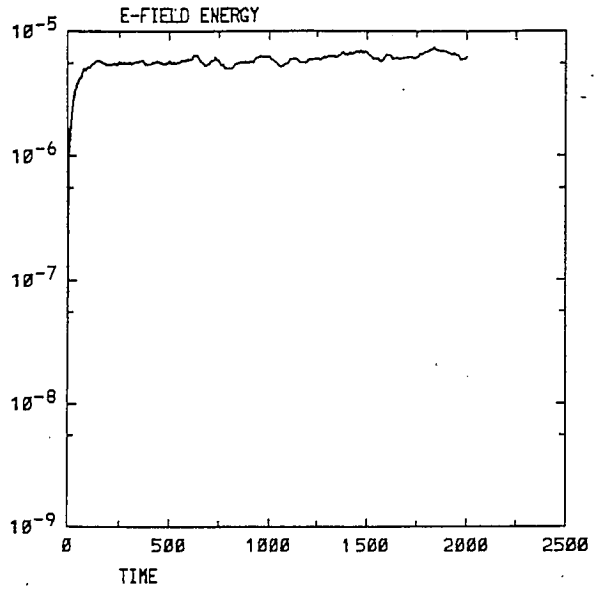
E-FIELD ENERGY
10^-5
10^-6
10^-7
10^-8
10^-9
0
500
1000
1500
2000
2500
TIME

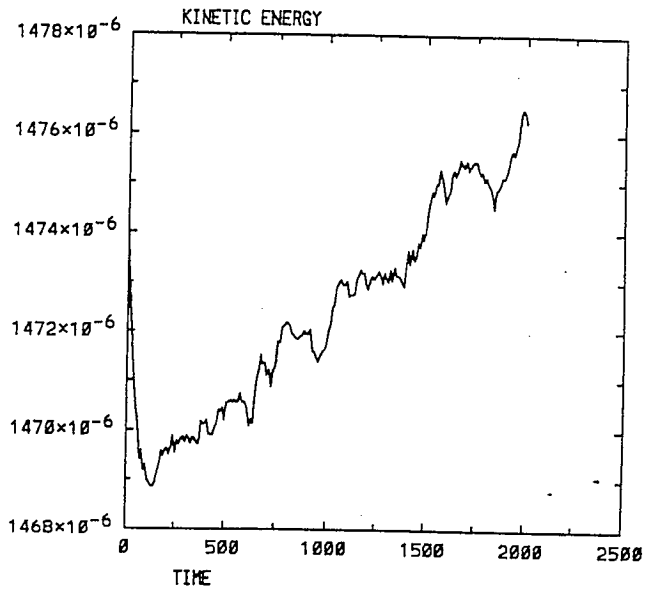
KINETIC ENERGY
1478x10^-6
1476x10^-6
1474x10^-6
1472x10^-6
1470x10^-6
1468x10^-6
0
500
1000
1500
2000
2500
TIME

b)

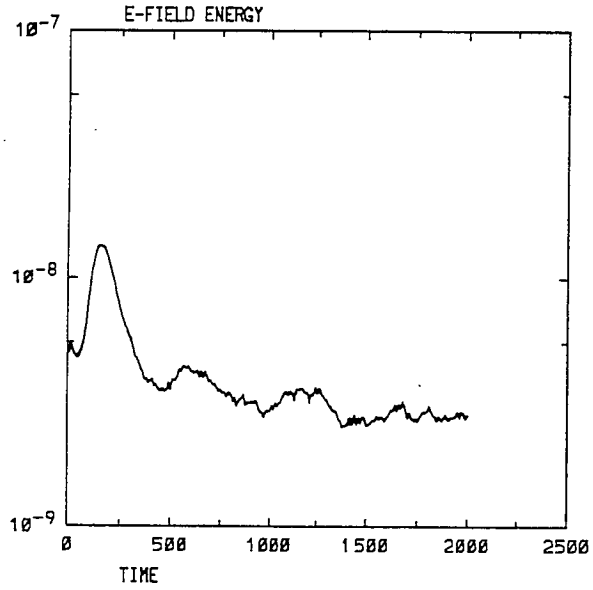
E-FIELD ENERGY
10^-7
10^-8
10^-9
0
500
1000
1500
2000
2500
TIME

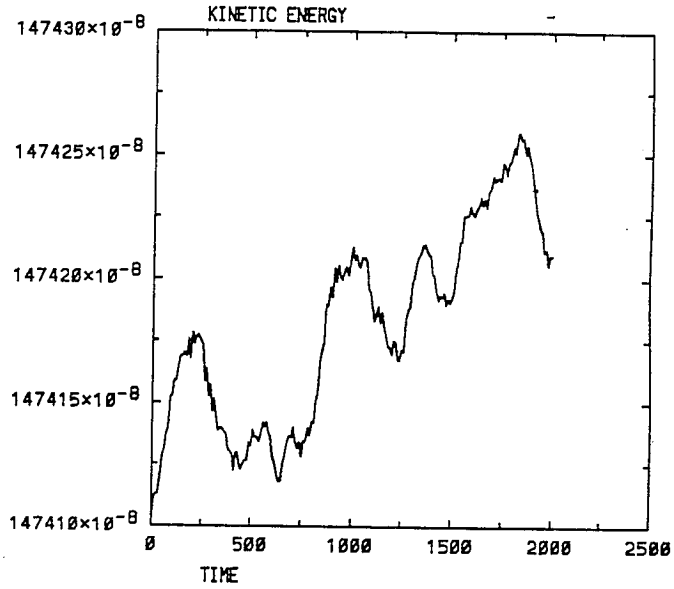
KINETIC ENERGY
147430x10^-8
147425x10^-8
147420x10^-8
147415x10^-8
147410x10^-8
0
500
1000
1500
2000
2500
TIME

c)

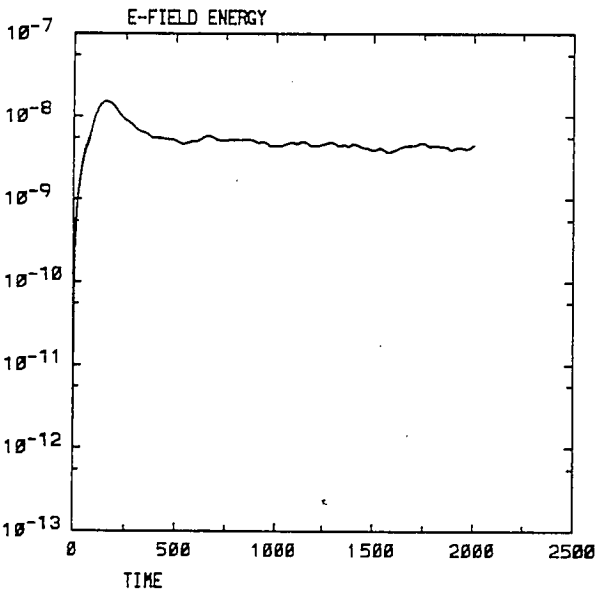
E-FIELD ENERGY
10^-7
10^-8
10^-9
10^-10
10^-11
10^-12
10^-13
0
500
1000
1500
2000
2500
TIME

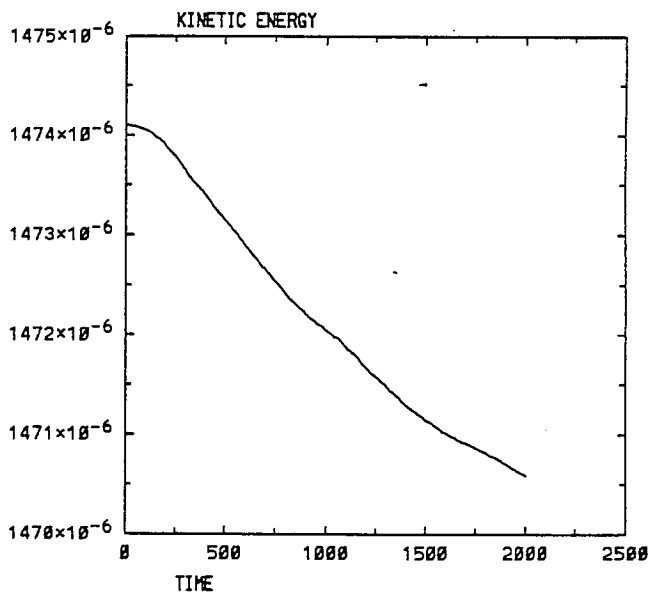
KINETIC ENERGY
1475x10^-6
1474x10^-6
1473x10^-6
1472x10^-6
1471x10^-6
1470x10^-6
0
500
1000
1500
2000
2500
TIME

Fig. 7